TU Delft

Delft University of Technology

Stability Analysis of Triple Active Bridge Converter with Hybrid Loads and Different Control Strategies

Yu, Haoyuan ; Zhang, Hanwen; Wang, Yanbo ; Qin, Zian; Chen, Zhe; Bauer, Pavol

DOI
10.1109/PEDG56097.2023.10215170

Publication date
2023

Document Version
Final published version

Published in
Proceedings of the 2023 IEEE 14th International Symposium on Power Electronics for Distributed Generation Systems (PEDG)

Citation (APA)
Yu, H., Zhang, H., Wang, Y., Qin, Z., Chen, Z., & Bauer, P. (2023). Stability Analysis of Triple Active Bridge Converter with Hybrid Loads and Different Control Strategies. In *Proceedings of the 2023 IEEE 14th International Symposium on Power Electronics for Distributed Generation Systems (PEDG)* (pp. 223-228). (PEDG 2023 - 2023 IEEE 14th International Symposium on Power Electronics for Distributed Generation Systems). IEEE. https://doi.org/10.1109/PEDG56097.2023.10215170

Important note
To cite this publication, please use the final published version (if applicable).
Please check the document version above.

Copyright
Other than for strictly personal use, it is not permitted to download, forward or distribute the text or part of it, without the consent of the author(s) and/or copyright holder(s), unless the work is under an open content license such as Creative Commons.

Takedown policy
Please contact us and provide details if you believe this document breaches copyrights.
We will remove access to the work immediately and investigate your claim.

This work is downloaded from Delft University of Technology.
For technical reasons the number of authors shown on this cover page is limited to a maximum of 10.

Green Open Access added to TU Delft Institutional Repository

'You share, we take care!' - Taverne project

https://www.openaccess.nl/en/you-share-we-take-care

Otherwise as indicated in the copyright section: the publisher is the copyright holder of this work and the author uses the Dutch legislation to make this work public.

2023 IEEE 14th International Symposium on Power Electronics for Distributed Generation Systems (PEDG) | 979-8-3503-2823-3/23/$31.00 ©2023 IEEE | DOI: 10.1109/PEDG56097.2023.10215170

Stability Analysis of Triple Active Bridge Converter with Hybrid Loads and Different Control Strategies

Haoyuan Yu
AAU Energy
Aalborg University
Aalborg, Denmark
hyu@energy.aau.dk

Hanwen Zhang
AAU Energy
Aalborg University
Aalborg, Denmark
hzha @energy.aau.dk

Yanbo Wang
AAU Energy
Aalborg University
Aalborg, Denmark
ywa@energy.aau.dk

Zian Qin
Electrical Sustainable Energy
Delft University of Technology
Delft, Netherlands
Z.Qin-2@tudelft.nl

Zhe Chen
AAU Energy
Aalborg University
Aalborg, Denmark
zch@energy.aau.dk

Pavol Bauer
Electrical Sustainable Energy
Delft University of Technology
Delft, Netherlands
P.Bauer@tudelft.nl

***Abstract*—This article investigates the stability of triple active bridge (TAB) converter with different types of loads. In this paper, port2 of TAB converter adopts voltage control to supply a constant power load (CPL), and port3 uses voltage control to supply a resistor or uses current control to supply a battery. Then, an extra element theorem-based (EET) modelling method based on the small signal model of the TAB converter is developed to derive the output impedance of different cases. The AC sweeping is implemented to validate the effectiveness of derivation. Furthermore, the impedance-based analysis method is applied to analyze the system stability. The analysis result shows that the instability issue caused by CPL at port2 can be suppressed by reducing the resistance load value at port3 or output current of port3. Simulation and experimental results are given to validate the stability analysis.**

Keywords—triple active bridge converter, extra element theorem, impedance-based analysis method, constant power load

I. Introduction

The application of multiport converters such as TAB converter has been paid increasingly concerns in power distribution system [1], aircraft [2],[3], and metro or railway traction power systems [4]-[6] due to the advantages of galvanic isolation and high power density.

A lot of work has addressed the controller design and power management of TAB converter connecting different loads or subsystems. For instance, traditional feed-forward decoupling matrix or polar coordinate decoupling matrix [7] are widely utilized to individually design the controller for each port. Since the operation point is not fixed, it is difficult to guarantee the singularity for every operating point. Furthermore, droop control is used to regulate the bus voltage of TAB converter and perform power management in aircraft [2]. Other methods such as fuzzy control and dynamic programming are used to achieve efficient power management in residential microgrids [8]. However, the stability of the TAB converter is slightly discussed.

For the two-port converter-based cascaded system, the oscillation phenomenon caused by the negative impedance of CPL is widely analyzed by small signal-based methods such as eigenvalue-based method [9] and impedance-based method [10]-[14]. In [10], the stability of the rectifier with a DAB converter is analyzed by identifying whether the ratio of the output impedance of rectifier to the input impedance of the DAB converter meets Nyquist criteria. It is also applied to analyze the stability of DAB converter with an input filter in [11]. And it is still effective for the entire system when two-port converter is acted as an interlinking converter to integrate multiple distribution power systems [12],[13].

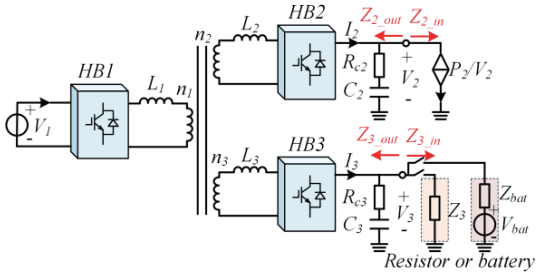

Fig. 1. The simplified structure of the proposed system.

For multi-port converter, the stability issue of the TAB converter with two CPLs under voltage control is investigated by the impedance-based method in our previous work [4]. It indicates that an increase of CPL power at one port will aggravate the instability issue at another port connecting with CPL. However, the instability issue of TAB converter is rarely discussed when one port of the TAB converter is connected to different types of loads and adopts different control methods.

To fill this gap, this article considers different types of loads at port3 as shown in Fig. 1. In case one, the port3 of TAB converter connects with a resistor, and voltage control is enabled to regulate bus voltage. In case two, the port3 connects with a battery, where current control is enabled to regulate output current of port3. The EET-based method, explained in [4], is used to obtain output impedance of port2 considering the load effect of port3. Then, the impedance-based analysis method is developed to investigate the impact of resistor variation and current variation on system stability.

The rest of this article can be organized as follows. In Section II, the small signal model of TAB converter and the output impedance by EET-based method are elaborated. In Section III, the impedance-based method is utilized to analyze system stability of different cases. In Section IV, simulation verification and experimental verification are implemented to validate the theoretical analysis. The conclusion is drawn in Section V.

II. System Description and Impendance Modelling

Fig. 1 shows the simplified structure of the TAB converter with hybrid loads, where the TAB converter is formed by a three-windings transformer and three H bridges (HB). As mentioned in Section I, port2 is connected with a CPL, and

Authorized licensed use limited to: TU Delft Library. Downloaded on August 31,2023 at 08:32:50 UTC from IEEE Xplore. Restrictions apply.

port3 is connected with a resistor in case one and a battery in case two.

A. Small signal model of the TAB converter

The TAB converter can be modelled as a three-port gyrator [4], which is shown in Fig. 2. The average transferred power of each port over one switching period can be obtained as (1) by the superposition principle [15],[16].

$$\begin{cases} P_1 = \dfrac{n_1 V_1 V_2}{2n_2 f_s L_{12}} d_{12}\left(1-|d_{12}|\right) + \dfrac{n_1 V_1 V_3}{2n_3 f_s L_{13}} d_{13}\left(1-|d_{13}|\right) \\ P_2 = \dfrac{n_1 V_1 V_2}{2n_2 f_s L_{12}} d_{12}\left(1-|d_{12}|\right) - \dfrac{n_1^2 V_2 V_3 d_{23}}{2n_2 n_3 f_s L_{23}}\left(1-|d_{23}|\right) \\ P_3 = \dfrac{n_1 V_1 V_3}{2n_3 f_s L_{13}} d_{13}\left(1-|d_{13}|\right) + \dfrac{n_1^2 V_2 V_3 d_{23}}{2n_2 n_3 f_s L_{23}}\left(1-|d_{23}|\right) \end{cases} \quad (1)$$

where f_s represents the switching frequency. L_{12}, L_{13} and L_{23} represent the equivalent leakage inductor of high-frequency transformer in Δ-connection. d_{12}, d_{13} and d_{23} represent the phase shifting ratio. n_1, n_2 and n_3 represent the winding turns of the transformer.

By linearization of (1) at a steady operation point, the small signal model of the TAB converter can be derived as (2), where the coefficients of G_{11}-G_{34} are given in Table I.

$$\begin{bmatrix} \hat{I}_1 \\ \hat{I}_2 \\ \hat{I}_3 \end{bmatrix} = \begin{bmatrix} 0 & G_{12} & G_{14} \\ G_{22} & 0 & G_{24} \\ G_{32} & G_{34} & 0 \end{bmatrix} \begin{bmatrix} \hat{V}_1 \\ \hat{V}_2 \\ \hat{V}_3 \end{bmatrix} + \begin{bmatrix} G_{11} & G_{13} \\ G_{21} & G_{23} \\ G_{31} & G_{33} \end{bmatrix} \begin{bmatrix} \hat{d}_{12} \\ \hat{d}_{13} \end{bmatrix} \quad (2)$$

B. The output impedance of the TAB converter with a resistor under voltage control

The EET-based method is applied to derive the uncoupled and coupled output impedance of the TAB converter, which is explained in [4]. According to Fig. 2, the voltage and current relationship at each port can be represented as (3).

$$\begin{cases} \left(\hat{I}_2 - \dfrac{\hat{V}_2}{Z_2} - \hat{I}_{load2}\right)\left(R_{c2} + \dfrac{1}{sC_2}\right) = \hat{V}_2 \\ \left(\hat{I}_3 - \dfrac{\hat{V}_3}{Z_3} - \hat{I}_{load3}\right)\left(R_{c3} + \dfrac{1}{sC_3}\right) = \hat{V}_3 \\ \hat{I}_2 = G_{21}\hat{d}_{12} + G_{22}\hat{V}_1 + G_{23}\hat{d}_{13} + G_{24}\hat{V}_3 \\ \hat{I}_3 = G_{31}\hat{d}_{12} + G_{32}\hat{V}_1 + G_{33}\hat{d}_{13} + G_{34}\hat{V}_2 \\ \hat{d}_{12} = \left(\hat{V}_{2\_ref} - \hat{V}_2\right)G_{v2} = -\hat{V}_2 G_{v2} \\ \hat{d}_{13} = \left(\hat{V}_{3\_ref} - \hat{V}_3\right)G_{v3} = -\hat{V}_3 G_{v3} \end{cases} \quad (3)$$

The uncoupled output impedance of port2 considering the effect of loads at port3 can be represented as (4) by the EET-based method.

$$Z_{2\_out}(s) = H_r(s)\left(1 + \frac{Z_N^3(s)}{Z_3(s)}\right) / \left(1 + \frac{Z_D^3(s)}{Z_3(s)}\right) \quad (4)$$

where the H_r(s) represents the impedance when the loads at port2 and port3 are neglected. Z_N^3(s) and Z_D^3(s) represent the null driving point impedance and driving point impedance seen from port3. H_r(s), Z_N^3(s) and Z_D^3(s) can be represented as (5)-(7), respectively.

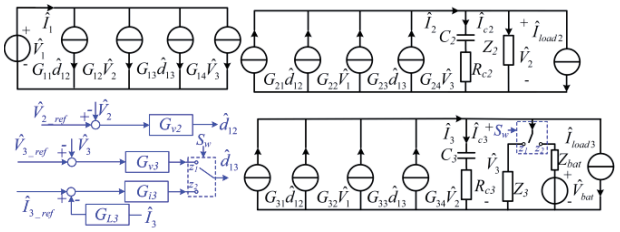

Fig. 2. The small signal model of the TAB converter

Table I The coefficients of the small signal model of the TAB converter

$$G_{11} = \frac{n_1 \bar{V}_2}{2n_2 f_s L_{12}}\left(1-2|\bar{d}_{12}|\right), G_{12} = \frac{n_1 \bar{d}_{12}}{2n_2 f_s L_{12}}\left(1-|\bar{d}_{12}|\right)$$

$$G_{13} = \frac{n_1 \bar{V}_3}{2n_3 f_s L_{13}}\left(1-2|\bar{d}_{13}|\right), G_{14} = \frac{n_1 \bar{d}_{13}}{2n_3 f_s L_{13}}\left(1-|\bar{d}_{13}|\right)$$

$$G_{22} = \frac{n_1 \bar{d}_{12}}{2n_2 f_s L_{12}}\left(1-|\bar{d}_{12}|\right), G_{23} = -\frac{n_1^2 \bar{V}_3}{2n_2 n_3 f_s L_{23}}\left(1-2|\bar{d}_{13}-\bar{d}_{12}|\right)$$

$$G_{24} = -\frac{n_1^2\left(\bar{d}_{13}-\bar{d}_{12}\right)}{2n_2 n_3 f_s L_{23}}\left(1-|\bar{d}_{13}-\bar{d}_{12}|\right), G_{31} = -\frac{n_1^2 \bar{V}_1}{2n_2 n_3 f_s L_{23}}\left(1-2|\bar{d}_{13}-\bar{d}_{12}|\right)$$

$$G_{32} = \frac{n_1 \bar{d}_{13}}{2n_3 f_s L_{13}}\left(1-|\bar{d}_{13}|\right), G_{34} = \frac{n_1^2\left(\bar{d}_{13}-\bar{d}_{12}\right)}{2n_2 n_3 f_s L_{23}}\left(1-|\bar{d}_{13}-\bar{d}_{12}|\right)$$

$$G_{21} = \frac{n_1 \bar{V}_1}{2n_2 f_s L_{12}}\left(1-2|\bar{d}_{12}|\right) + \frac{n_1^2 \bar{V}_3}{2n_2 n_3 f_s L_{23}}\left(1-2|\bar{d}_{13}-\bar{d}_{12}|\right)$$

$$G_{33} = \frac{n_1 \bar{V}_1}{2n_3 f_s L_{13}}\left(1-2|\bar{d}_{13}|\right) + \frac{n_1^2 \bar{V}_2}{2n_2 n_3 f_s L_{23}}\left(1-2|\bar{d}_{13}-\bar{d}_{12}|\right)$$

$$\frac{1}{H_r(s)} = \frac{sC_2}{sC_2R_{c2}+1} + \frac{\left(G_{23}-G_{24}\right)\left(G_{34}-G_{31}G_{v2}\right)}{\dfrac{sC_3}{sR_{c3}C_3+1} + G_{33}G_{v3}} + G_{21}G_{v2} \quad (5)$$

$$\frac{1}{Z_D^3(s)} = \frac{sC_3}{sR_{c3}C_3+1} + \frac{\left(G_{31}G_{v2}-G_{34}\right)\left(G_{24}-G_{23}G_{v3}\right)}{\dfrac{sC_2}{sR_{c2}C_2+1} + G_{21}G_{v2}} + G_{33}G_{v3} \quad (6)$$

$$Z_N^3(s) = \frac{sC_3R_{c3}+1}{sC_3 + G_{33}G_{v3}\left(sC_3R_{c3}+1\right)} \quad (7)$$

The coupled output impedance of port2, which considers the effect of the load at port2, is obtained as (8).

$$Z_{2\_out\_c} = Z_{2\_out} / \left(1 + Z_{2\_out}/Z_2\right) \quad (8)$$

Fig. 3(a) shows the AC sweeping results in PLECS, where port2 and port3 connect with a 20Ω resistor. The parameters of the TAB converter and control system are given in Table II. It can be seen from Fig. 3(a) that the analysis results agree with the sweeping results. It also validates the effectiveness of the derivation of uncoupled output impedance.

C. The output impedance of the TAB converter with a battery under current control

In this situation, port3 is connected to a battery and current control is enabled to regulate the output current. The voltage and current relationship at each port can be represented as (9).

Authorized licensed use limited to: TU Delft Library. Downloaded on August 31,2023 at 08:32:50 UTC from IEEE Xplore. Restrictions apply.

Table II The parameters of the TAB converter

Parameter	Value	Parameter	Value
Bus voltage $V_{1\text{-}3}$ (V)	200	Winding turns n_1:n_2:n_3	1:1:1
Capacitor $C_{2,3}$ (uF)	820	Leakage inductor $L_{1\text{-}3}$ (uH)	50
Switch frequency f_s (Hz)	10k	ESR of capacitor $R_{c2,c3}$ (Ω)	0.01
Battery voltage V_{bat} (V)	195	Internal resistance Z_{bat} (Ω)	0.05
Current filter ω_c (rad/s)	6283	Damping factor ζ	0.707
Voltage controller $G_{v2,v3}$: 2e-4+0.1005/s			
Current controller G_{i3}: 0.01+2.5133/s			
Current filter: G_{L3}: $\omega_c^2/(s^2+2\omega_c\zeta s+\omega_c^2)$			

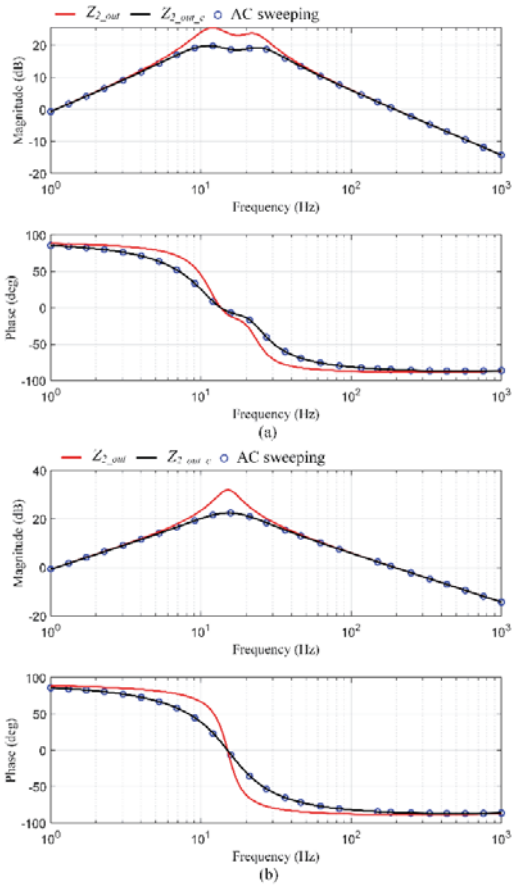

Fig. 3. The output impedance of port2. (a) Port3 connects with a resistor. (b) Port3 connects with a battery.

$$\begin{cases} \left(\hat{I}_2-\dfrac{\hat{V}_2}{Z_2}-\hat{I}_{load2}\right)\left(R_{c2}+\dfrac{1}{sC_2}\right)=\hat{V}_2 \\ \left(\hat{I}_3-\dfrac{\hat{V}_3-\hat{V}_{bat}}{Z_{bat}}-\hat{I}_{load3}\right)\left(R_{c3}+\dfrac{1}{sC_3}\right)=\hat{V}_3 \\ \hat{I}_2=G_{21}\hat{d}_{12}+G_{22}\hat{V}_1+G_{23}\hat{d}_{13}+G_{24}\hat{V}_3 \\ \hat{I}_3=G_{31}\hat{d}_{12}+G_{32}\hat{V}_1+G_{33}\hat{d}_{13}+G_{34}\hat{V}_2 \\ \hat{d}_{12}=\left(\hat{V}_{2\_ref}-\hat{V}_2\right)G_{v2}=-\hat{V}_2G_{v2} \\ \hat{d}_{13}=\left(\hat{I}_{3\_ref}-G_{L3}\hat{I}_3\right)G_{i3}=-\hat{I}_3G_{L3}G_{i3} \end{cases} \tag{9}$$

Similarly, the uncoupled output impedance of port2 in this case can be represented as (10) by the EET-based method.

$$Z_{2\_out1}(s)=H_{r1}(s)\left(1+\frac{Z_{N1}^3(s)}{Z_{bat}(s)}\right)/\left(1+\frac{Z_{D1}^3(s)}{Z_{bat}(s)}\right) \tag{10}$$

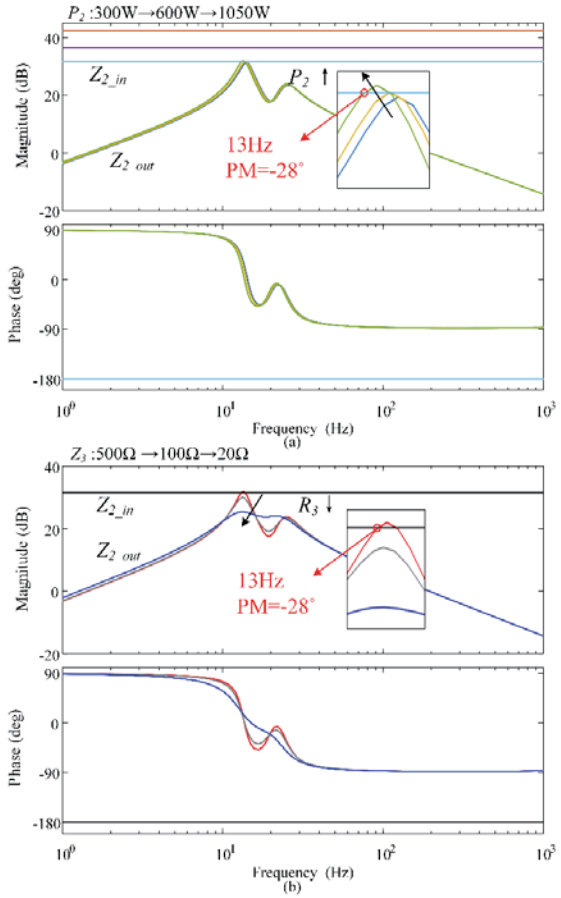

Fig. 4. The frequency characteristic of port2 when port3 connects with a resistor. (a) Impedance comparison when P_2 is increased. (b) Impedance comparison when the value of resistor Z_3 is decreased.

$$\frac{1}{H_{r1}(s)}=\frac{sC_2}{sC_2R_{c2}+1}+G_{21}G_{v2}+G_{23}G_{L3}G_{i3}\cdot\frac{G_{34}-G_{31}G_{v2}}{1+G_{33}G_{L3}G_{i3}} -G_{24}\left(\frac{G_{34}-G_{31}G_{v2}}{1+G_{33}G_{L3}G_{i3}}\right)/\left(\frac{sC_3}{sC_3R_{c3}+1}+\frac{1}{Z_{bat}}\right) \tag{11}$$

The null driving point impedance Z_{N1}^3(s) and driving point impedance Z_{D1}^3(s) can be obtained as (12) and (13).

$$\frac{1}{Z_{D1}^3(s)}=\frac{sC_3}{sR_{c3}C_3+1}+\frac{1}{Z_{bat}} -\frac{(G_{34}-G_{31}G_{v2})a_2}{1+G_{33}G_{L3}G_{i3}-(G_{34}-G_{31}G_{v2})b_2} \tag{12}$$

$$Z_{N1}^3(s)=\frac{sC_3R_{c3}Z_{bat}+Z_{bat}}{sC_3(R_{c3}+Z_{bat})+1} \tag{13}$$

Fig. 3(b) shows the AC sweeping results in PLECS when I_{3_Ref} is 10A. It can be seen that the analysis results agree with the sweeping results.

III. Impedance-based Stability Analysis

In this section, the impedance-based analysis method is adopted to analyze the stability of the proposed system. The system stability can be identified by whether the phase margin (PM) is higher than zero degree. The PM can be represented as (14).

Authorized licensed use limited to: TU Delft Library. Downloaded on August 31,2023 at 08:32:50 UTC from IEEE Xplore. Restrictions apply.

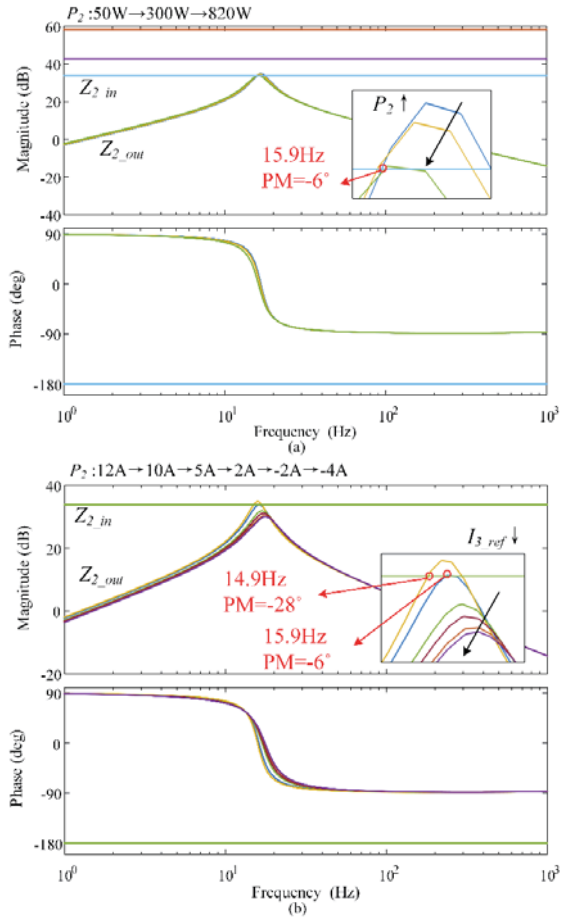

Fig. 5. The frequency characteristic of port2 when port3 connects with a resistor. (a) Impedance comparison when P_2 is increased. (b) impedance comparison when the value of resistor Z_3 is decreased.

$$PM = 180° - \left| \angle Z_{2\_out} - \angle Z_{2\_in} \right| \tag{14}$$

If the PM is higher than zero degree, the system is stable. Otherwise, the system would be unstable.

A. *Stability analysis of the TAB converter when Port3 connects with a resistor*

Fig. 4(a) shows the frequency characteristic of Port2 output impedance (Z_{2_out}) and input impedance (Z_{2_in}) when Z_3 is kept at 500Ω. It can be seen that there exist two intersection points between Z_{2_out} and Z_{2_in} when P_2 is increased to 1050W. The frequency and phase margin of the left intersection point is 13Hz and -28 degrees. It indicates that the system would become unstable under the situation that P_2 is 1050W and Z_3 is 500Ω. Also, an oscillation phenomenon with 13Hz can be seen.

Fig. 4(b) shows the frequency characteristic of Z_{2_out} and Z_{2_in} when P_2 is kept at 1050W and Z_3 is decreased to 20Ω from 500Ω. It can be seen from Fig. 4(b) that the magnitude of Z_{2_out} in the frequency domain is reduced when Z_3 is decreased to 100Ω and 20Ω. There is no intersection point between Z_{2_out} and Z_{2_in}, which indicates that the system would be stable.

Therefore, when the TAB converter adopts voltage control to regulate the bus voltage of port3, a small resistor connected with port3 of the TAB converter can mitigate the oscillation phenomenon at port2.

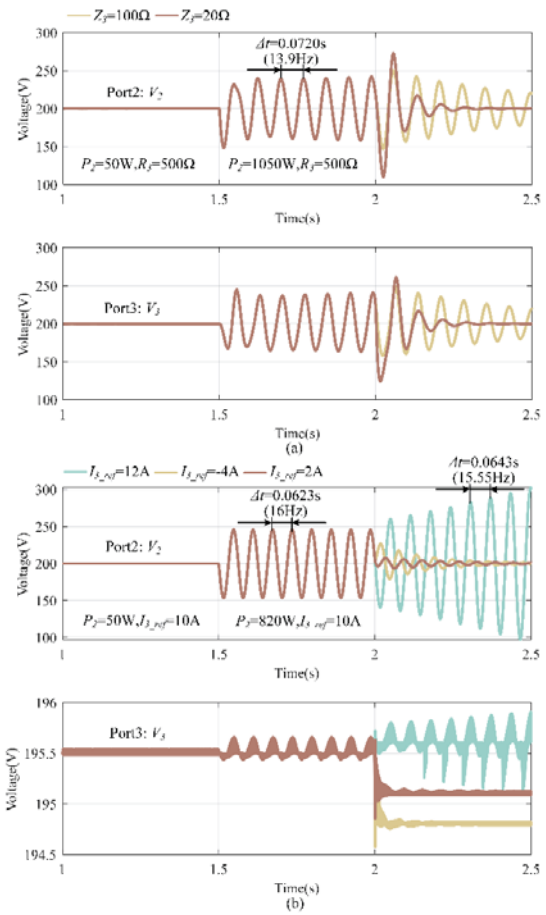

Fig. 6. Simulation results. (a) Port3 connects with a resistor. (b) Port3 connects with a battery.

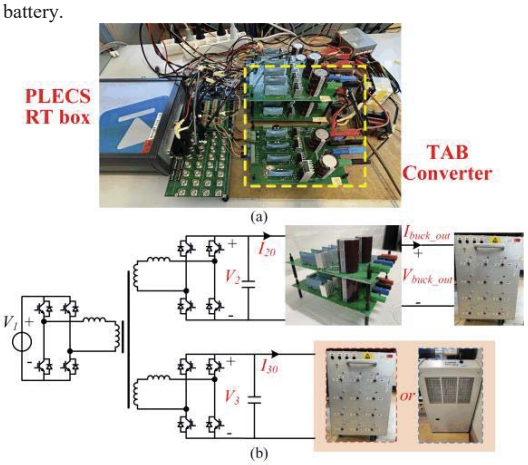

Fig. 7. The laboratory prototypes.

B. *Stability analysis of the TAB converter when Port3 connects with a battery*

Fig. 5(a) shows the frequency characteristic of Z_{2_out} and Z_{2_in} when I_{3_ref} is kept at 10A. There exist two intersection points when P_2 is increased to 820W. The phase margin of the left intersection point is -6 degrees, which indicates that the system would be unstable with 15.9Hz oscillation. Fig. 5(b) shows the frequency characteristic of Z_{2_out} and Z_{2_in} when P_2 is kept at 820W and I_{3_ref} is decreased to -4A from 12A. The

Authorized licensed use limited to: TU Delft Library. Downloaded on August 31,2023 at 08:32:50 UTC from IEEE Xplore. Restrictions apply.

Table III The parameters of the experimental prototype

Parameter	Value	Parameter	Value
Bus voltage V_1(V)	100	Winding turns n_1:n_2:n_3	2:1:1
Bus voltage $V_{2,3}$(V)	50	Leakage inductor L_{12}(uH)	5.27
Switch frequency f_s (Hz)	10k	Leakage inductor L_{13}(uH)	5.52
Capacitor $C_{2,3}$(uF)	410	Leakage inductor L_{23}(uH)	3.31
Voltage controller $G_{v2,v3}$: 2e-3+0.63/s			
Current controller G_{i3}: 1e-3+0.32/s			

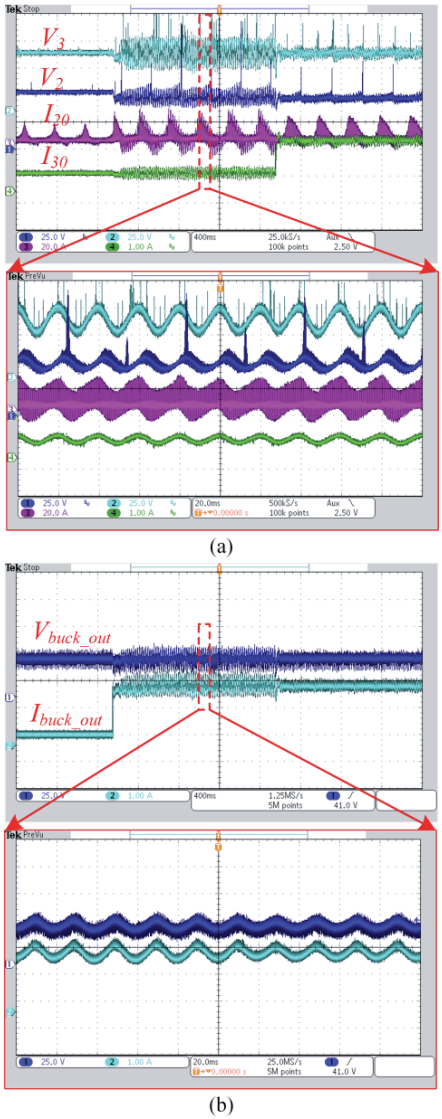

Fig. 8. The experimental verification of TAB converter with buck converter and resistor. (a) The waveform of bus voltage and current. (b) The waveform of buck converter.

magnitude of Z_{2_out} in the frequency domain is reduced gradually when I_{3_ref} is decreased to 5A, 2A, -2A and -4A, which indicates that the system would be stable.

Therefore, when port3 adopts voltage control to supply a resistor load, the system will become more stable if port3 supplies more power for the load. However, when port3 adopts current control to supply a battery load, the system will become more stable only if port3 reduces the output current or absorbs energy from the battery.

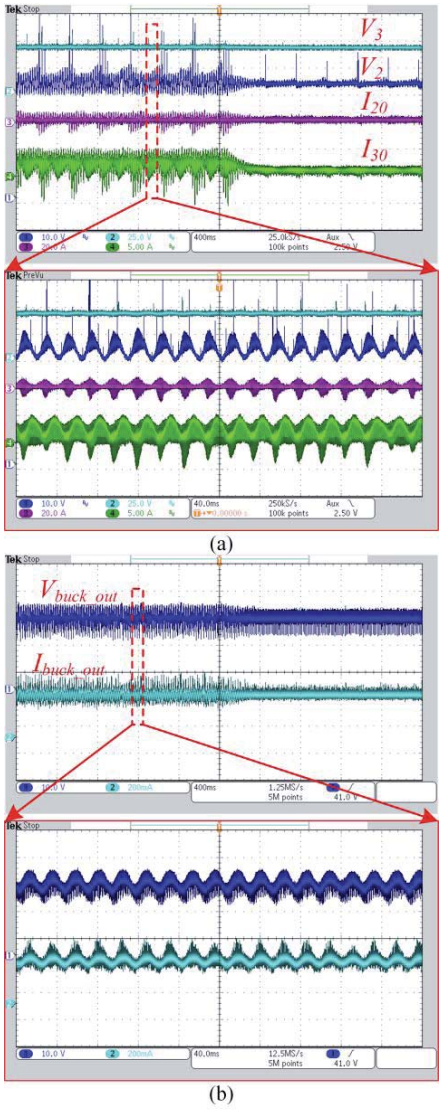

Fig. 9. The experimental verification of TAB converter with buck converter and grid emulator. (a) the waveform of bus voltage and current. (b) the waveform of buck converter.

IV. Simulation and Experimental Verification

A. Simulation verification

Fig. 6(a) shows the simulation results when port3 adopts voltage control to supply a resistor. It can be seen that the system occurs oscillation phenomenon when P_2 is increased to 1050W at 1.5s. The oscillation frequency is 13.9Hz, which agrees with the analysis in Fig. 4(a). Then, the resistor Z_3 is decreased to 100Ω and 20Ω at 2s. It can be seen from Fig. 6(a) that a 20Ω resistor can mitigate the oscillation phenomenon with more fast response than a 100Ω resistor, which agrees with the stability analysis in Fig. 4(b).

Fig. 6(b) shows the simulation results when port3 is enabled by current control to supply a battery. It can be seen that the oscillation phenomenon is caused when P_2 is increased to 820W and I_{3_ref} is kept at 10A at 1.5s, where the oscillation frequency is 16Hz. It agrees with the analysis in Fig. 5(a). When I_{3_ref} is increased to 12A, the oscillation phenomenon becomes more obvious, and the oscillation frequency is decreased to 15.55Hz. However, when I_{3_ref} is

Authorized licensed use limited to: TU Delft Library. Downloaded on August 31,2023 at 08:32:50 UTC from IEEE Xplore. Restrictions apply.

decreased to 2A and -4A, the oscillation phenomenon is mitigated at 2s, which agrees with the analysis in Fig. 5(b).

B. Experimental verification

Fig. 7 shows the experimental setup of the TAB converter, where the control system is implemented by PLECS RT Box. In this work, the CPL is emulated by a buck converter with a resistor and voltage control is implemented to maintain the constant load voltage. The battery is emulated by a grid emulator (CA MX30) operated in DC mode. The parameters of this prototype are given in Table III.

Fig. 8 shows the experimental verification when port2 connects with a buck converter and port3 connects with a resistor, where Fig. 8(a) shows the bus voltage and current of the TAB converter and Fig. 8(b) shows the voltage and current of the buck converter at the load side. The bus voltage of V_2 and V_3 is 50V at normal operation and the output voltage of buck converter (V_{buck_out}) is kept at 40V. It can be found that the low-frequency oscillation phenomenon is amplified since the output current of the buck converter (I_{buck_out}) is increased. Then, the power of port3 is increased by adding a parallel resistor. It can be seen that the oscillation phenomenon is mitigated. Therefore, the power increase of port3 can alleviate the oscillation phenomenon caused by CPL at port2 when voltage control is applied for port3.

Fig. 9 shows the experimental verification when port2 connects with a buck converter and port3 connects with a grid emulator. It can be seen that an oscillation phenomenon is caused when the output current from port3 to grid emulator (I_{30}) is 3A. Then, it can be found that the oscillation phenomenon is mitigated when I_{30} is decreased to 1A. It indicates that the power reduction of port3 can alleviate the oscillation phenomenon caused by the CPL at port2 current control is adopted for port3.

V. Conclusion

This paper presents an extra element theorem-based modelling method to derive output impedance of TAB converter when a resistor with voltage control is connected to port3 or a battery with current control is connected to port3. The AC sweeping results validate the effectiveness of the proposed impedance model, and the impedance-based method is adopted to analyze the system stability of different cases. Simulation and experiments are given to validate the stability analysis. The simulation and verification results show that the oscillation issue occurs when the power of CPL at port2 is increased. The oscillation problem can be eliminated by reducing the resistor value in port3 when voltage control is enabled to regulate the bus voltage of port3. Also, the oscillation problem can be eliminated by reducing the output current of port3 when current control is implemented at port3.

References

[1] S. Zhao, Y. Chen, S. Cui, B. J. Mortimer and R. W. De Doncker, "Three-Port Bidirectional Operation Scheme of Modular-Multilevel DC–DC Converters Interconnecting MVDC and LVDC Grids," *IEEE Trans. Power Electron*., vol. 36, no. 7, pp. 7342-7348, July 2021.

[2] C. Gu et al., "A Multiport Power Conversion System for the More Electric Aircraft," *IEEE Trans. Transp. Electrific*., vol. 6, no. 4, pp. 1707-1720, Dec. 2020.

[3] B. Karanayil, M. Ciobotaru and V. G. Agelidis, "Power Flow Management of Isolated Multiport Converter for More Electric Aircraft," *IEEE Trans. Power Electron*., vol. 32, no. 7, pp. 5850-5861, July 2017.

[4] H. Yu, Y. Wang, H. Zhang and Z. Chen, "Impedance Modelling and Stability Analysis of Triple Active Bridge Converter-Based Renewable Electricity-Hydrogen-Integrated Metro DC Traction Power System," *IEEE Trans. Ind. Electron*., early access, doi: 10.1109/TIE.2023.3237898.

[5] H. Yu, Y. Wang, and Z. Chen, "A Renewable Electricity-Hydrogen-Integrated Hybrid DC Traction Power System," in *Proc. 2021 SPEC*, Kigali, Rwanda, 2021, pp. 1-6.

[6] F. Ma, X. Wang, L. Deng, Z. Zhu, Q. Xu and N. Xie, "Multiport Railway Power Conditioner and Its Management Control Strategy With Renewable Energy Access," *IEEE J. Emerg. Sel. Topics Power Electron*., vol. 8, no. 2, pp. 1405-1418, June 2020.

[7] S. Okutani, A. Nishi, P. -Y. Huang and Y. Kado, "Polar Coordinate Decoupling Power Flow Control for Triple Active Bridge Converter," in *Proc. 2019 ICDCM*, Matsue, Japan, 2019, pp. 1-5.

[8] M. Jafari, Z. Malekjamshidi, J. Zhu and M. -H. Khooban, "A Novel Predictive Fuzzy Logic-Based Energy Management System for Grid-Connected and Off-Grid Operation of Residential Smart Microgrids," *IEEE J. Emerg. Sel. Topics Power Electron*., vol. 8, no. 2, pp. 1391-1404, June 2020.

[9] Y. Wang, X. Wang, F. Blaabjerg, and Z. Chen, "Harmonic Instability Assessment Using State-Space Modeling and Participation Analysis in Inverter-Fed Power Systems," *IEEE Trans. Ind. Electron*., vol. 64, no. 1, pp. 806-816, Jan. 2017

[10] F. Feng, X. Zhang, J. Zhang, and H. B. Gooi, "Stability Enhancement via Controller Optimization and Impedance Shaping for Dual Active Bridge-Based Energy Storage Systems," *IEEE Trans. Ind. Electron*., vol. 68, no. 7, pp. 5863-5874, Jul. 2021.

[11] Y. Guan, Y. Xie, Y. Wang, Y. Liang, and X. Wang, "An Active Damping Strategy for Input Impedance of Bidirectional Dual Active Bridge DC–DC Converter: Modeling, Shaping, Design, and Experiment," *IEEE Trans. Ind. Electron*., vol. 68, no. 2, pp. 1263-1274, Feb. 2021

[12] P. Pan et al., "An Impedance-Based Stability Assessment Methodology for DC Distribution Power System With Multivoltage Levels," *IEEE Trans. Power Electron*., vol. 35, no. 4, pp. 4033-4047, Apr. 2020.

[13] M. Leng, G. Zhou, H. Li, G. Xu, F. Blaabjerg and T. Dragičević, "Impedance-Based Stability Evaluation for Multibus DC Microgrid Without Constraints on Subsystems," *IEEE Trans. Power Electron*., vol. 37, no. 1, pp. 932-943, Jan. 2022.

[14] H. Yu, Y. Wang, and Z. Chen, "Impedance-based Stability Analysis of Metro Traction Power System Considering Regenerative Braking," in *Proc. 2020 IPEMC2020-ECCE Asia*, Nanjing, China, 2020, pp. 224-229.

[15] S. Falcones, R. Ayyanar, and X. Mao, "A DC–DC Multi-port-Converter-Based Solid-State Transformer Integrating Distributed Generation and Storage," *IEEE Trans. Power Electron*., vol. 28, no. 5, pp. 2192-2203, May 2013.

[16] C. Zhao, S. D. Round, and J. W. Kolar, "An Isolated Three-Port Bidirectional DC-DC Converter With Decoupled Power Flow Management," *IEEE Trans. Power Electron*., vol. 23, no. 5, pp. 2443-2453, Sept. 2008.

Authorized licensed use limited to: TU Delft Library. Downloaded on August 31,2023 at 08:32:50 UTC from IEEE Xplore. Restrictions apply.